SUPLEMENTAL INFORMATION

Atmospheric CO_2 estimates for the Miocene to Pleistocene based on foraminiferal $\delta^{11}B$ at Ocean Drilling Program Sites 806 and 807 in the Western Equatorial Pacific

Maxence Guillermic[1,2], Sambuddha Misra[3,4], Robert Eagle[1,2], Aradhna Tripati [1,2]

[1]Department of Atmospheric and Oceanic Sciences, Department of Earth, Planetary, and Space Sciences, Center for Diverse Leadership in Science, Institute of the Environment and Sustainability, University of California – Los Angeles, Los Angeles, CA 90095 USA

[2]Laboratoire Géosciences Océan UMR6538, UBO, Institut Universitaire Européen de la Mer, Rue Dumont d'Urville, 29280, Plouzané, France

[3]The Godwin Laboratory for Palaeoclimate Research, Department of Earth Sciences, University of Cambridge, UK

[4]Indian Institute of Science, Centre for Earth Sciences, Bengaluru, Karnataka 560012, India

Supplemental Methods

S1. Potential contamination

We found no evidence for contamination of TE (including Mg/Ca) arising from the presence of silicate minerals or Mn-Fe-Oxide coatings. Contamination of samples by silicate minerals was monitored using Fe/Mg ratios. Samples with Fe/Mg > 0.1 mol/mol are typically rejected due to potential contamination by silicate minerals (Barker et al., 2003). Our samples have an average Fe/Mg of 0.034 ± 0.07 mol/mol (2 SD, n=106), indicating that silicate minerals have been efficiently removed during our cleaning. Contamination by clays was monitored using Ti/Ca no correlations were found between Ti/Ca and Mg/Ca (R^2=0.0066) or with B/Ca (R^2=0.0237). Contamination by Mn-Fe oxides is detected using Mn/Ca ratios and Fe/Ca ratios. Our samples have Mn/Ca ratios of 0.12 ± 0.11 mmol/mol (2 SD, n=108) consistent with previous published data of cleaned samples (Wara et al., 2005). No correlations was observed between Mg/Ca and Fe/Ca (R^2=0.0841) or between Mg/Ca and Mn/Ca (R^2=0.0161). No significant correlation was observed between B/Ca and Mn/Ca (R^2=0.0011) or B/Ca and Fe/Ca (R^2=0.0132) ratios.

S2. Calculations of temperature, salinity, pH, and pCO_2

Analyses of $\delta^{11}B$, $\delta^{18}O$ and elemental ratios (eg., Mg/Ca, B/Ca) were used to reconstruct the chemical and physical properties of seawater over the last 17 My of the Western Equatorial Pacific (Fig. 2).

S2.1. Salinity reconstruction

Salinity was reconstructed using the relative sea level (RSL) reconstruction from Stap et al. (2017) and equation S1:

$$S=S_{modern}/3800*(3800+RSL) \qquad \textbf{eq. S1}$$

S_{modern} is the modern salinity corresponding to the depth habitat of the foraminifera at the site of interest. The depths used were 125 m for *T. sacculifer* and 80m for *G. ruber* (Rickaby et al., 2005; Guillermic et al., 2020). At Site 806, values for S_{modern} of 35.38 was used for *T. sacculifer* and 35.01 was used for *G. ruber*. At Site 807, a value of 35.05 was used for *T. sacculifer*.

S2.2. Temperature

Paleotemperatures were calculated using Mg/Ca ratios of planktic foraminifera. A number of factors have been shown to impact Mg/Ca ratios and calculated paleotemperature. Factors identified in prior studies include salinity and pH effects on Mg/Ca, seawater Mg/Ca ratios, cleaning methodology, dissolution, and basin-specific equations, as discussed in more detail below. Below we describe some of the prior work that was factored into the regional mono-specific equations we used for calculating temperature from Mg/Ca.

S2.2.1. Prior work showing evidence for salinity and pH effects on Mg/Ca-T

Studies have found that Mg/Ca ratios in foraminifera are impacted by salinity (Nürnberg et al., 1996; Hönisch et al., 2013) and pH or [CO_3^{2-}] (Russell et al., 2004; Kisakürek et al., 2008; Evans et al., 2016; Gray et al., 2018; Gray and Evans, 2019). Based on culture experiments, Gray and Evans (2019) reported impacts of both salinity and pH on *G. ruber* but only a salinity effect on *T. sacculifer*, and derived the following equations:

$$\text{SST}\ (T.sacculifer) = (Ln(\frac{Mg}{Ca}test) - 0.054 * (S - 35) + 0.24)/0.062 \quad \textbf{eq. S2}$$

$$\text{SST}\ (G.ruber) = (Ln(\frac{Mg}{Ca}test - 0.036 * (S - 35) + 0.87 * (\text{pH} - 8) + 0.03)/0.064 \quad \textbf{eq. S3}$$

S2.2.2. Prior work showing evidence for variations in Mg/Ca ratios of seawater

Over timescales of 10^6-10^7 years, Mg/Ca_{sw} can vary. Evidence from evaporites, carbonate veins, fossil corals and models suggests that seawater Mg/Ca_{sw} ratios have varied through time with variations of ~3 mol/mol (Horita et al., 2002; DeFantle and Paolo, 2006; Coggon et al., 2011; Brennan et al., 2013; Gothman et al., 2015). These studies do not agree on the timing of changes in Mg/Ca_{sw}. To correct for secular variations in Mg/Ca_{sw} we used the approach of O'Brien et al. (2014), theoretical work from Evans and Muller, (2012), and the Mg/Ca_{sw} fourth polynomial equation from Sosdian et al., (2020) derived from calcite veins (Coggon et al., 2010; Rausch et al., 2013), fluid inclusions (Brennan et al., 2013; Horita et al., 2002), echinoderms (Dickson, 2002), and larger benthic foraminifera (Evans et al., 2018). The equations we utilized are adapted from Dekens et al. (2002):

$$\text{SST}\ (T.sacculifer) = (Ln(\frac{Mg}{Ca}test * \frac{Mg^H}{Ca}sw_{t0}) \quad - Ln(0.37 * \frac{Mg^H}{Ca}sw_t))/0.09 + 0.36 * C + D$$

eq. S4

$$\text{SST}\ (G.ruber) = (Ln(\frac{Mg}{Ca}test * \frac{Mg^H}{Ca}sw_{t0}) \quad - Ln(0.37 * \frac{Mg^H}{Ca}sw_t))/0.09 + 0.61 * C + D \quad \textbf{eq. S5}$$

Specifically H refers to the power components of the power law relationship between the Mg partition coefficient and Mg/Ca_{sw}, with a value of 0.41 for *T. sacculifer* (Delaney et al., 1985) which we also assume is the same for *G. ruber*. C is the depth of the site. D refer to a basin-specific offset, which is 2 °C for *T. sacculifer* and 2.9 °C for *G. ruber* for the Pacific Ocean, (Table S1).

S2.2.3. Prior work on reductive cleaning effects on Mg/Ca

The use of a reductive step in cleaning has been shown to lower Mg/Ca_{test} ratios in planktic (Barker et al., 2003; Bian et al., 2010; Johnstone et al., 2016) and benthic foraminifera (Yu et al., 2007a), and contribute to offsets between studies using different methodologies. A decrease in Mg/Ca_{test} of 6-9% was reported for *T. sacculifer* by Bian et al. (2010), and of 5% by Johnstone et al. (2016). A decrease of 4% was reported for *G. ruber* by Johnstone et al. (2016).

S2.2.4. Mg/Ca-SST equations used for this study

Based on the above equations from Gray and Evans (2019) (eq. S2 and S3), we incorporated a term to account for changes in the Mg/Ca ratio of seawater, and based on results from Dekens et al., (2002) we incorporated two terms to account for dissolution (C) and basin-specific offsets (D), and used an iterative approach for our calculations to account for pH effect on *G. ruber (*Gray and Evans, 2019). The equations we used are:

$$\text{SST}\ (T.sacculifer) = \frac{Ln\left((\frac{Mg}{Ca}test * 1.05 * \frac{\frac{Mg^H}{Ca}sw_{t0}}{\frac{Mg^H}{Ca}sw_t}\right) - 0.054 * (S-35) + 0.24}{0.062} + 0.36 * C + 2.0 \quad \textbf{eq. S6}$$

$$\text{SST}\ (G.ruber) = \frac{Ln\left(\frac{Mg}{Ca}test * 1.05 * \frac{\frac{Mg^H}{Ca}sw_{t0}}{\frac{Mg^H}{Ca}sw_t}\right) - 0.036 * (S-35) + 0.87 * (\text{pH}-8) + 0.03}{0.064} + 0.61 * C + 2.9 \quad \textbf{eq. S7}$$

With H being the power components of the power relationship between the Mg partition coefficient and Mg/Ca_{sw}, 0.41 for *T. sacculifer* (Delaney et al., 1985). We use the same value

for *G. ruber*. C is the depth of the core (km). In order to take the impact of reductive cleaning into account we applied a decrease of 5% for *G. ruber* and *T. sacculifer* (Bian et al., 2010 and Johnstone et al., 2016).

Given evidence for a pH effect on Mg/Ca-SST calibration for *G. ruber*, we used an iterative approach for our calculations, following Gray and Evans, (2019). Up to 4 iterations were needed to achieve a difference in SST with the previous iteration of <0.05°C and a difference in pH of <0.001. For this iterative approach, we first calculate pH_1 from foraminiferal $\delta^{11}B$, then calculate SST_1 from pH_1, then calculate pH_2 with SST_1, and then repeat.

S2.3. $\delta^{11}B_{borate}$ from $\delta^{11}B_{carbonate}$

The use of $\delta^{11}B$ in foraminiferal carbonate to calculate seawater $\delta^{11}B_{borate}$, and derived pH and pCO_2 values**,** has been shown to accurately replicate pCO_2 records independently determined from ice cores and using oceanographic data, if several factors are taken into account (Chalk et al., 2017; Guillermic et al., 2020). These factors include mono-specific calibrations, size fraction or shell weight, basin, and water depth. In order to accurately reconstruct seawater pH (and pCO_2) from $\delta^{11}B$ of foraminifera, mono-specific calibrations are needed to convert $\delta^{11}B_{carbonate}$ to $\delta^{11}B_{borate}$. Recent culture and field-based calibrations have refined the sensitivities of $\delta^{11}B_{carbonate}$ to $\delta^{11}B_{borate}$ for different foraminiferal species (Henehan et al., 2016; Raitzsch et al., 2018; Guillermic et al., 2020). For *T. sacculifer* and *G. ruber*, the sensitivities of $\delta^{11}B_{carbonate}$ to $\delta^{11}B_{borate}$ are 0.82 and 0.58, respectively (Raitzsch et al., 2018; Guillermic et al., 2020). As with Mg/Ca, the intercepts are prone to large uncertainties and are commonly adjusted based on core-top data, in order to yield the expected pre-industrial pH or pCO_2 value at the site being examined (Chalk et al., 2017; Sosdian et al., 2018). The rationale for this correction is the impact of the depth habitat on microenvironment pH and subsequent $\delta^{11}B_{carbonate}$ (Hönisch and Hemming, 2004; Guillermic et al., 2020) and/or preferential dissolution of gametogenic calcite (Ni et al., 2007). It is also possible that these offsets may reflect observed size effects on *G. ruber* as well as *T. sacculifer* (Henehan et al., 2013; Hönisch et al., 2019). For *T. sacculifer*, a relationship between shell size and $\delta^{11}B_{carbonate}$ has been observed in the WEP (Hönisch and Hemming, 2004; Ni et al., 2007). Hönisch and Hemming, (2004) also reported that values for the 515-865 µm size fraction yielded values of 21.76 ‰, and determined a size-fraction specific relationship. Here, we modify this approach to develop a shell-weight specific relationship:

147 $$\text{Size offset (‰)} = 21.76 - (0.06522 * \text{Weight/shell (µg)} + 17.38) \quad \textbf{eq. S8}$$

148 We adapted the equation for *T. sacculifer* from Guillermic et al. (2020):

149 $$\delta^{11}B_{borate} = [(\delta^{11}B_{T.\ sacculifer} + \text{Size offset}) - 4.09\ (\pm 0.86)] / 0.83\ (\pm 0.48) \quad \textbf{eq. S9}$$

150 Due to the lack of coretop measurements for *G. ruber* from this study, we selected three
151 control points at Marine isotope stages (MIS) 30, 37 and 39 (Lisiecky and Raymo, 2005)
152 times when both *T. sacculifer* and *G. ruber* where measured to determine appropriate offsets
153 for both Mg/Ca and $\delta^{11}B$ that yield (Table S1 and S2) the best agreement between the
154 species. This was used to adapt the equation from Guillermic et al. (2020) for *G. ruber*:
155
156 $$\delta^{11}B_{borate} = [(\delta^{11}B_{G.\ ruber} + 2.0) - 9.11\ (\pm 0.73)] / 0.58\ (\pm 0.91) \quad \textbf{eq. S10}$$
157
158 **S2.4. Constants**

159 Temperature, salinity and pressure were used to calculate the different dissociation
160 constants and parameters. We used K_1, K_2 from Lueker et al. (2000), K_B from Dickson,
161 (1990), KSO_4 from Dickson, (1990), KF from Peres and Fraga, (1987) and total boron from
162 Lee et al. (2010).
163
164 **S2.5. pH calculations**

165 The quantitative estimation of pH using downcore $\delta^{11}B_{carbonate}$ requires: 1) calculations
166 of the borate isotopic composition of seawater ($\delta^{11}B_{borate}$), 2) constraints on the secular
167 variation of the boron isotopic composition of seawater ($\delta^{11}B_{seawater}$), 3) the fractionation
168 factor (α) between $B(OH)_3$ and $B(OH)_4^-$ and 4) the calculations of acid/base equilibrium
169 constants based temperature, salinity and pressure. To translate our $\delta^{11}B$ measurements to pH,
170 we used the following relationship (Hemming and Hanson, 1992):
171

172 $$pH = pK_B^* - \log\left(\frac{\delta^{11}B_{seawater} - \delta^{11}B_{borate}}{\delta^{11}B_{seawater} - \alpha * \delta^{11}B_{borate} - \varepsilon}\right) \quad \textbf{eq. S11}$$

173

174 pK_B^* is the dissociation constant between the two boron species (8.5975 at 25 °C and a
175 salinity of 35 psu, Dickson, 1990). A fractionation between $B(OH)_3$ and $B(OH)_4^-$ (ε) of 27.2
176 ± 0.6 ‰ was empirically determined by Klochko et al. (2006) in seawater and confirmed
177 independently using a different method by Nir et al. (2015).

A few studies have attempted to reconstruct secular variations of $\delta^{11}B_{seawater}$ (Lemarchand et al., 2000; Foster et al., 2012; Raitzsch and Hönisch, 2013; Greenop et al., 2017). For our work, we first compared different scenarios (Fig. 3). These scenarios are modeled values of $\delta^{11}B_{seawater}$ based on constraints on the boron budget from Lemarchand et al. (2000), a second modeled history that assumed changes in seawater pH from Raitzsch and Hönisch (2013), and a third scenario that also considered constraints on pH gradients from $\delta^{13}C$ measurements published by Greenop et al. (2017).

S2.6. pCO_2 calculations

The carbonate system has two degrees of freedom, meaning that if two parameters of the carbonate system are known all the others can be calculated. For this study, we utilized pH calculated using $\delta^{11}B_{borate}$, and total alkalinity (TA) as a second parameter that are shown in Fig. 3-4. We used four different alkalinity scenarios for our calculations (Constant alkalinity; Tyrell and Zeebe, 2004; Ridgwell and Zeebe, 2005; and Caves et al. 2016). For all calculations, we used the MS excel program "CO_2sys" version 2.3 from Pierrot et al. (2006). pH and TA, temperature, salinity were used to determined pCO_2 in ppm.

S2.7. Error propagation for temperature (T), pH and pCO_2

The main source of uncertainty in reconstructed pCO_2 comes from the errors in pH. Table S3 summarizes the sensitivity of pH and pCO_2 to different variables. The individual uncertainties were propagated in quadrature to combined uncertainties for temperature (δT), pH (δpH) and pCO_2 (δpCO_2) (eq. S12, S13, S14, S15, S16 and S17). Minimum and maximum propagated uncertainties were derived separately for pH and pCO_2. δpCO_2 (A) is the full uncertainty propagation, δpCO_2 (B) is the uncertainty propagation without taking into account the $\delta^{11}B_{sw}$. Both are shown in the figures and discussed below.

$$\delta T_{G.\ ruber} = \sqrt{(\delta T\_Mg/Ca)^2 + (\delta T\_Salinity)^2 + (\delta T\_pH)^2} \quad \textbf{eq. S12}$$

$$\delta T_{T.\ sacculifer} = \sqrt{(\delta T\_Mg/Ca)^2 + (\delta T\_Salinity)^2} \quad \textbf{eq. S13}$$

$$\delta pH\ (A) = \sqrt{(\delta pH\_Temperature)^2 + (\delta pH\_Salinity)^2 + (\delta pH\_\delta^{11}B_{sw})^2 + (\delta pH\_\delta^{11}B_{carbonate})^2}$$

eq. S14

$$\delta pH\ (B) = \sqrt{(\delta pH\_Temperature)^2 + (\delta pH\_Salinity)^2 + (\delta pH\_\delta^{11}B_{carbonate})^2}$$ **eq. S15**

$$\delta pCO_2\,(A) = \sqrt{\begin{array}{c}(\delta pCO_2\_Temperature)^2 + (\delta pCO_2\_Salinity)^2 + (\delta pCO_2\_\delta^{11}B_{sw})^2 + \\ (\delta pCO_2\_\delta^{11}B_{carbonate})^2 + (\delta pCO_2\_Alkalinity)^2\end{array}}$$ e**q. S16**

$$\delta pCO_2\,(B) = \sqrt{\begin{array}{c}(\delta pCO_2\_Temperature)^2 + (\delta pCO_2\_Salinity)^2 + \\ (\delta pCO_2\_\delta^{11}B_{carbonate})^2 + (\delta pCO_2\_Alkalinity)^2\end{array}}$$ e**q. S17**

With for example, "δpCO_2_Temperature" being the uncertainty in pCO_2 due to temperature.

Figures

Figure S1: Evaluation of pCO_2 reconstruction for the past 0.8 million year in the Western Equatorial Pacific compared to benthic oxygen isotope data. **A.** Benthic $\delta^{18}O$ (blue line – stack from Lisiecki and Raymo, 2005; black line – compilation from Zachos et al., 2008). **B to E**, colored is indicating the site (filled light blue=806, filled dark blue=807), symbols represent the species (circle=*T. sacculifer* and triangle=*G. ruber*), filled grey squares are recalculated data based on Sosdian et al. (2018) at site 872. Reconstructed pCO_2 (ppm) using boron-based pH and alkalinity from Caves et al. (2016), data presented are from this study. Propagated uncertainties are given by eq. S17 for the dark blue envelope, while the light blue envelope are the uncertainties calculated based on eq. S16 (taking into account uncertainty on $\delta^{11}B_{seawater}$). Solid black line represents data from ice cores (Bereiter et al., 2015). **B.** Colored data from this study. **C.** Colored data from this study and pCO_2 from original publications. **D.** Colored data from this study and data recalculated by Rae et al. (2021). **E.** Colored data from this study and data recalculated by Sosdian et al. (2018).

Figure S2: Evaluation of pCO_2 reconstruction for the past 22 million years in the Western Equatorial Pacific compared to benthic oxygen isotope data. **A.** Benthic $\delta^{18}O$ (blue line – stack from Lisiecki and Raymo, 2005; black line – compilation from Zachos et al., 2008). **B to E**, colored is indicating the site (filled light blue=806, filled dark blue=807), symbols represent the species (circle=*T. sacculifer* and triangle=*G. ruber*), filled grey squares are recalculated data based on Sosdian et al. (2018) at site 872. Reconstructed pCO_2 (ppm) using boron-based pH and alkalinity from Caves et al. (2016), data presented are from this study. Propagated uncertainties are given by eq. S17 for the dark blue envelope, while the light blue envelope are the uncertainties calculated based on eq. S16 (taking into account uncertainty on $\delta^{11}B_{seawater}$). Solid black line represents data from ice cores (Bereiter et al., 2015). **B.** Colored data from this study. **C.** Colored data from this study and pCO_2 from original publications. **D.** Colored data from this study and data recalculated by Rae et al. (2021). **E.** Colored data from this study and data recalculated by Sosdian et al. (2018).

Figure S3: $\delta^{18}O$ records from ODP Sites 806 (benthic from Lear et al., 2003, 2015, dark red line; planktic from Medina-Elizalde and Lea, 2005, black line) and 807 (Zhang et al., 2007, dark green line) as well as benthic stack LR05 (Lisiecki and Raymo, 2005, grey line).

Figure S4: Cross plot for the last 0.8 Myr of $pCO_{2T.\ sacculifer}$ from this study and pCO_2_ice core (from ice core compilation, Bereiter et al., 2015). **A.** Open blue symbols (this study), open triangles (Chalk et al., 2017) and green squared (Hönisch et al., 2009), unit of pCO_2 are the same as original publications. Lines are linear regressions from each study (blue for this study; grey for Chalk et al., 2017; green for Hönisch et al., 2009), blue dotted line is a Deming regression for the data in our study with bootstrap (n=1000) taking into account both x and y uncertainties (p = 0.25), ice core CO_2 error calculated based 2 SD on ± 1 ky on the age determined from age model and boron based pCO_2 error is calculated based on error propagation eq. S17, outputs of the regression are presented in Table S6; our data present more variability than Chalk et al. (2017) or Hönisch et al. (2009). **B**. Data from this study, ODP Site 806 (light blue) and ODP Site 807 (dark blue) to assess no significant difference in variability between Sites.

Tables

Table S1: Analytical data and reconstructed parameters for ODP Sites 806 and 807.

Table S2: Control points for a 2‰ offset used for *G. ruber*.

Table S3: Comparison of the control points reconstructions between *T. sacculifer* and *G. ruber* for MIS 30, 37 and 39, using different offsets (see text).

Table S4: Sensitivity tests for reconstructed pH and pCO_2 (G17, Caves-16), all results are given as the minimum and maximum variation (%) observed in our data.

Table S5: Boron isotopes standard reproducibility.

Table S6: CamWuellestorfi, X/Ca standard reproducibility.

Table S7: Output of linear and Deming regressions made on the comparison between ice core and boron isotopes derived pCO_2.

Table S2: Control points for a 2‰ offset used for *G. ruber*

	Species	Sample					mcd	mbsf	Shell Wt	Age	SST	error	Salinity	TA	pH	error(1) up	pCO_2	error(1) up	error(1) down
									(µg)	(Ma)	(°C)	(°C)	(psu)	(µmol/kg)	(total scale)		(ppm)	(ppm)	(ppm)
MIS 30	*G. ruber*	806	B	3	5	6	8	22.06	22.06	16.1	1.046	26.2	1.8	35.3	2241	8.16	0.09	258	74	57
	T. sacculifer	806	B	3	5	31	33	22.31	22.31	18.2	1.048	26.0	0.9	35.6	2230	8.28	0.08	174	47	37
MIS 37	*G. ruber*	806	B	4	1	71	73	26.21	26.21	17.0	1.240	26.4	1.9	35.1	2230	8.09	0.09	318	96	72
	T. sacculifer	806	B	4	1	56	58	26.06	26.06	22.2	1.233	29.8	0.9	35.6	2228	8.08	0.09	308	91	69
MIS 39	*G. ruber*	806	B	4	1	131	133	26.81	26.81	16.1	1.267	27.8	1.9	35.5	2228	8.09	0.09	320	95	71
	T. sacculifer	806	B	4	1	146	148	26.96	26.96	24.0	1.274	27.8	0.9	35.6	2219	8.07	0.09	319	97	72

Table S3: Comparaison of the control points reconstructions between *T. sacculifer* and *G.ruber* for MIS 30, 37 and 39, using different offsets (see text).

	1.8 ‰ offset			**1.85 ‰ offset**			**2.0 ‰ offset**			**2.1 ‰ offset**		
	MIS 30	**MIS 37**	**MIS 39**	**MIS 30**	**MIS 37**	**MIS 39**	**MIS 30**	**MIS 37**	**MIS 39**	**MIS 30**	**MIS 37**	**MIS 39**
ΔpCO_2 (ppm)	105	37	26	100	31	20	86	13	2	77	1	-10
ΔpH (tot scale)	-0.14	-0.02	-0.01	-0.14	-0.01	-0.003	-0.12	0.01	0.02	-0.11	0.02	0.03
ΔT (°C)	-0.02	-3.75	-0.36	0.06	-3.65	-0.27	0.31	-3.39	-0.005	0.47	-3.21	0.17

Table S4: Sensitivity tests for reconstructed pH and pCO_2 (G17, Caves-16), all results are given as the minimum and maximum variation (%) observed in our data

	Salinity	**Temperature**	**$\delta^{11}B_{carbonate}$**	**$\delta^{11}B_{seawater}$**	**Alkalinity**
pH (*G. ruber*)	0.07%	0.2-0.3%	0.2-0.5 %	0.8-1.6 %	NA
pH (*T. sacculifer*)	0.07-0.08 %	0.12-0.13 %	0.1-0.5 %	0.8-1.4 %	NA
pCO_2 (*G. ruber*)	0.8-1.5 %	0.02-1.5 %	5-11 %	19-25 %	5 %
pCO_2 (*T. sacculifer*)	0.8-1.4 %	0.02-0.7 %	3-12 %	19-27 %	5-7 %

NA: non determined parameter

Table S5: Boron isotopes standard reproducibility.

Standard	$\delta^{11}B_1$ (‰)	$2SD_{AE121}$	n_{AE121}	$\delta^{11}B_2$ (‰)	$2SD_{AE121}$	n_{AE121}
NEP1	25.36	0.36	11	25.32	0.36	11
NEP2	25.21	0.25	11	25.22	0.25	11
NEP3	25.00	0.30	12	24.70	0.30	12
NEP4	25.40	0.21	11	25.32	0.21	11
NEP5	25.33	0.21	11	25.22	0.21	11
NEP7	25.26	0.26	15	25.39	0.26	15
NEP8	26.15	0.26	15	25.97	0.26	15
NEP9	26.09	0.26	15	26.09	0.26	15
NEP10	26.22	0.26	15	26.29	0.26	15
NEP11	26.19	0.26	15	26.21	0.26	15
NEP12	26.12	0.26	15	26.13	0.26	15
NEP13	26.00	0.26	15	26.04	0.26	15
NEP15	26.02	0.29	12			
NEP16	25.86	0.29	12			
NEP17	25.83	0.19	3	25.49	0.33	8
NEP18	25.72	0.19	3	26.03	0.33	8
NEP19	26.48	0.33	8	26.06	0.33	8
NEP20	25.82	0.27		25.50	0.27	
NEP21	25.42	0.15	3			
NEP22	25.28	0.29	8			
NEP23	25.32	0.15	3	25.34	0.29	8
NEP24	25.27	0.29	8	25.47	0.29	8
NEP25	25.54	0.22	6			
NEP26	25.86	0.22	4	25.95	0.22	4
NEP27	26.16	0.22	6	26.42	0.22	6
NEP28	25.77	0.25	9			
NEP29	25.37	0.22	4			
NEP30	25.88	0.25	9			
NEP31	25.46	0.22	4			
NEP32	25.93	0.25	9			
NEP33	26.41	0.22	4	26.21	0.22	4
JCP-1-1	24.07	0.10				
JCP-1-2	24.17	0.11		24.17	0.10	
JCP-1-3	24.01	0.11				
JCP-1-4	23.92	0.26				
JCP-1-5	24.03	0.26		24.05	0.39	
JCP-1-6	24.18	0.36		24.16	0.36	

Standard	Average $\delta^{11}B$	2SD	n	
NEP	25.72	0.79	31	This sudy
NEP	26.20	0.88	27	Holcomb et al. 2015
NEP	25.80	0.89	6	Sutton et al. 2017
JCP-1	24.06	0.19	6	This study
JCP-1	24.37	0.32	57	Holcomb et al. 2015
JCP-1	24.42	0.28	7	Sutton et al. 2017

*Some data in this table are also presented in Guillermic et al. 2021 because data were collected at the same period

281
282

Table S6: CamWuellestorfi, X/Ca standard reproducibility

Sample	Li/Ca µmol/mol	B/Ca µmol/mol	Mg/Ca mmol/mol	Sr/Ca mmol/mol	Cd/Ca µmol/mol	Ba/Ca µmol/mol	U/Ca nmol/mol	Mn/Ca µmol/mol	Fe/Ca mmol/mol
CamWuellerstorfi	16.0	204	1.22	1.31	0.26	4.6	43	67	0.04
CamWuellerstorfi	16.3	209	1.24	1.32	0.28	4.6	45	69	0.04
CamWuellerstorfi	16.3	209	1.23	1.31	0.26	4.6	44	77	0.04
CamWuellerstorfi	16.0	207	1.23	1.32	0.28	4.6	44	74	0.04
CamWuellerstorfi	16.4	210	1.23	1.32	0.27	4.6	42	74	0.04
CamWuellerstorfi	16.0	208	1.24	1.31	0.26	4.6	42	74	0.04
CamWuellerstorfi	16.6	213	1.23	1.32	0.28	4.6	44	74	0.04
CamWuellerstorfi	16.0	203	1.22	1.32	0.26	4.6	41	72	0.04
CamWuellerstorfi	16.1	205	1.22	1.32	0.27	4.6	42	76	0.04
CamWuellerstorfi	16.2	204	1.22	1.32	0.27	4.6	41	72	0.04
CamWuellerstorfi	16.1	205	1.22	1.32	0.27	4.5	41	71	0.04
CamWuellerstorfi	15.8	204	1.21	1.32	0.27	4.6	42	73	0.04
CamWuellerstorfi	16.1	206	1.22	1.32	0.27	4.6	42	68	0.04
CamWuellerstorfi	16.0	207	1.22	1.32	0.26	4.6	43	66	0.04
CamWuellerstorfi	15.9	203	1.21	1.32	0.27	4.6	42	68	0.04
CamWuellerstorfi	16.3	201	1.22	1.31	0.22	4.6	41	66	0.03
CamWuellerstorfi	16.1	203	1.22	1.32	0.23	4.6	42	67	0.03
CamWuellerstorfi	16.4	202	1.22	1.32	0.23	4.6	42	69	0.04
CamWuellerstorfi	16.3	202	1.22	1.31	0.22	4.6	41	68	0.04
CamWuellerstorfi	16.6	202	1.22	1.31	0.23	4.6	44	67	0.03
CamWuellerstorfi	16.6	205	1.22	1.31	0.24	4.5	42	66	0.03
CamWuellerstorfi	16.1	204	1.22	1.31	0.22	4.6	40	67	0.03
CamWuellerstorfi	16.4	204	1.22	1.31	0.23	4.6	43	67	0.03
CamWuellerstorfi	16.4	202	1.22	1.32	0.23	4.6	43	64	0.03
CamWuellerstorfi	16.2	198	1.22	1.31	0.31	4.6	42	74	0.04
CamWuellerstorfi	16.4	200	1.22	1.30	0.30	4.6	43	73	0.04
CamWuellerstorfi	16.2	201	1.23	1.31	0.31	4.7	43	74	0.04
CamWuellerstorfi	16.3	198	1.22	1.31	0.30	4.6	42	73	0.04
CamWuellerstorfi	16.6	200	1.23	1.30	0.30	4.6	42	73	0.04
CamWuellerstorfi	16.5	198	1.22	1.31	0.31	4.6	44	74	0.04
CamWuellerstorfi	16.1	201	1.22	1.30	0.32	4.7	43	74	0.04
CamWuellerstorfi	16.5	197	1.25	1.31	0.29	4.9	43	72	0.04
CamWuellerstorfi	16.6	197	1.25	1.32	0.29	4.8	44	74	0.04
CamWuellerstorfi	16.8	196	1.25	1.32	0.29	4.9	44	72	0.04
CamWuellerstorfi	17.0	198	1.25	1.32	0.28	4.9	44	71	0.04
CamWuellerstorfi	16.8	198	1.25	1.31	0.29	4.9	44	73	0.04
CamWuellerstorfi	16.5	198	1.25	1.31	0.29	4.9	43	72	0.04
CamWuellerstorfi	16.7	200	1.24	1.32	0.29	4.9	43	74	0.04
CamWuellerstorfi	16.9	202	1.24	1.31	0.29	4.9	43	74	0.04
Average	16.3	203	1.23	1.31	0.27	4.7	43	71	0.04
2SD	0.6	8	0.02	0.01	0.05	0.2	2	7	0.01
n	39	39	39	39	39	39	39	39	39

*Some data in this table are also presented in Guillermic et al. 2021 because data were collected at the same period

283

Table S7: Output of linear and Deming regressions made on the comparison between ice core and boron isotopes derived pCO_2.

Linear regression

Bootstrap (n=1000)

	Output	Bias	SD
Slope	0.73	0.06	0.51
Intercept	63	-11,85	118
R2	0.09	0.03	0.09
p-value	0.25	0.04	0.23

Deming regression

Bootstrap (n=1000)

	Output	Bias	SD
Slope	6.6	1.19	49.8
Intercept	-1273.0	-261	11501.0
R2	*NA*	*NA*	*NA*
p-value	0.25	0.03	0.23

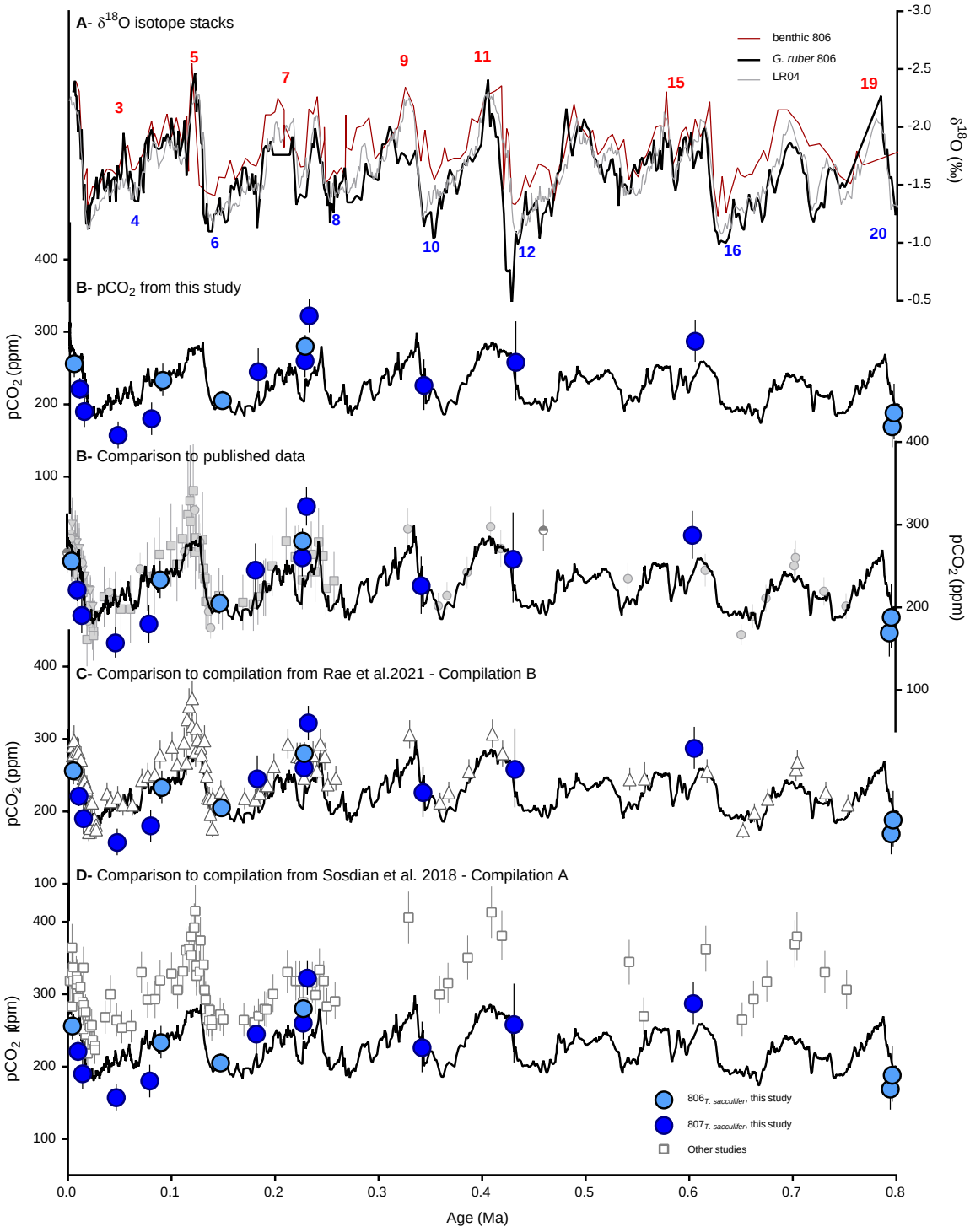
A- δ18O isotope stacks
benthic 806
G. ruber 806
LR04
δ18O (‰)
B- pCO2 from this study
pCO2 (ppm)
B- Comparison to published data
C- Comparison to compilation from Rae et al.2021 - Compilation B
D- Comparison to compilation from Sosdian et al. 2018 - Compilation A
806T. sacculifer, this study
807T. sacculifer, this study
Other studies
Age (Ma)

Figure S1

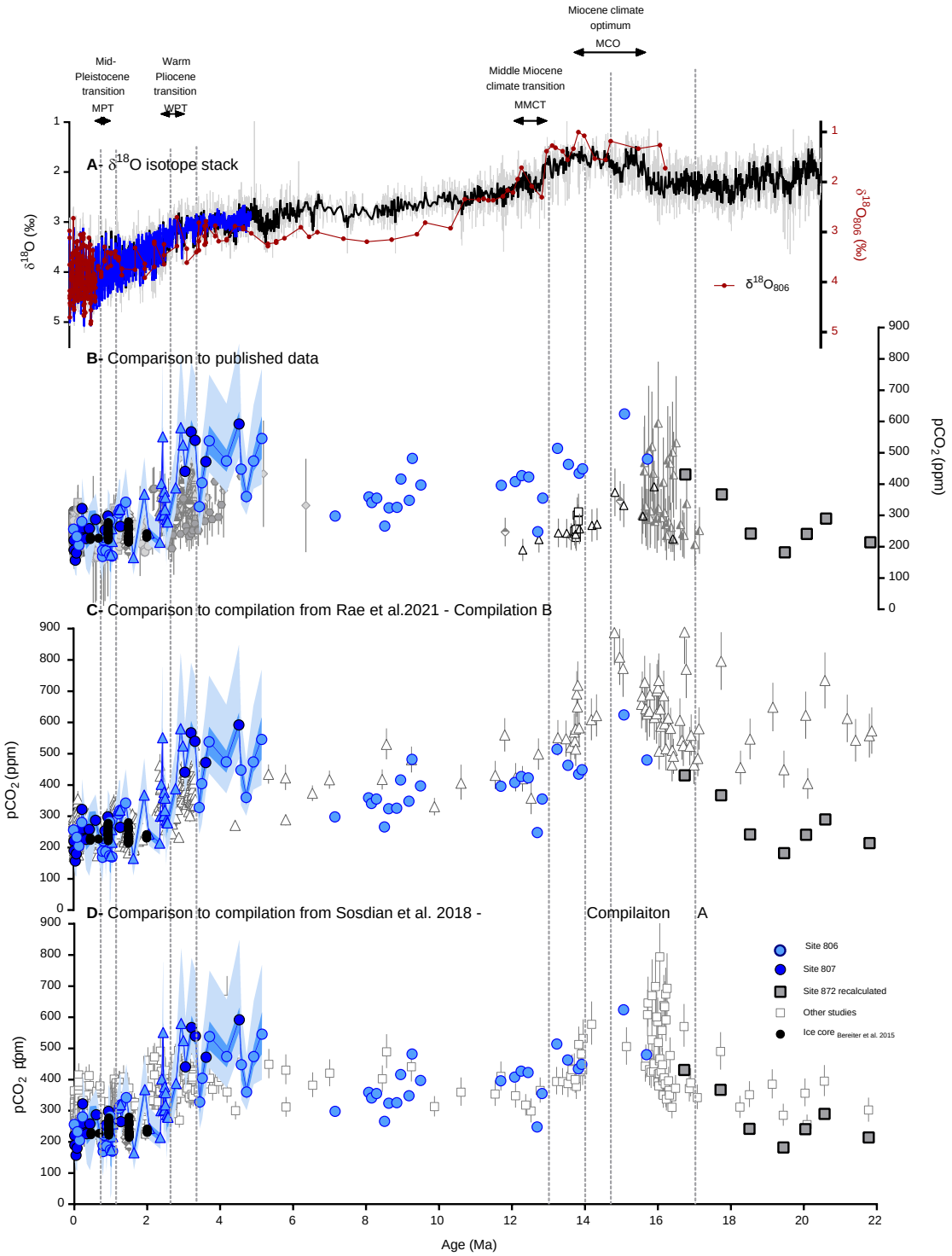
Miocene climate optimum
MCO
Mid-Pleistocene transition
MPT
Warm Pliocene transition
WPT
Middle Miocene climate transition
MMCT
A- δ18O isotope stack
δ18O (‰)
δ18O806 (‰)
δ18O806
B- Comparison to published data
pCO2 (ppm)
C- Comparison to compilation from Rae et al.2021 - Compilation B
pCO2 (ppm)
D- Comparison to compilation from Sosdian et al. 2018 - Compilaiton A
pCO2 (ppm)
Site 806
Site 807
Site 872 recalculated
Other studies
Ice core Bereiter et al. 2015
Age (Ma)

Figure S2

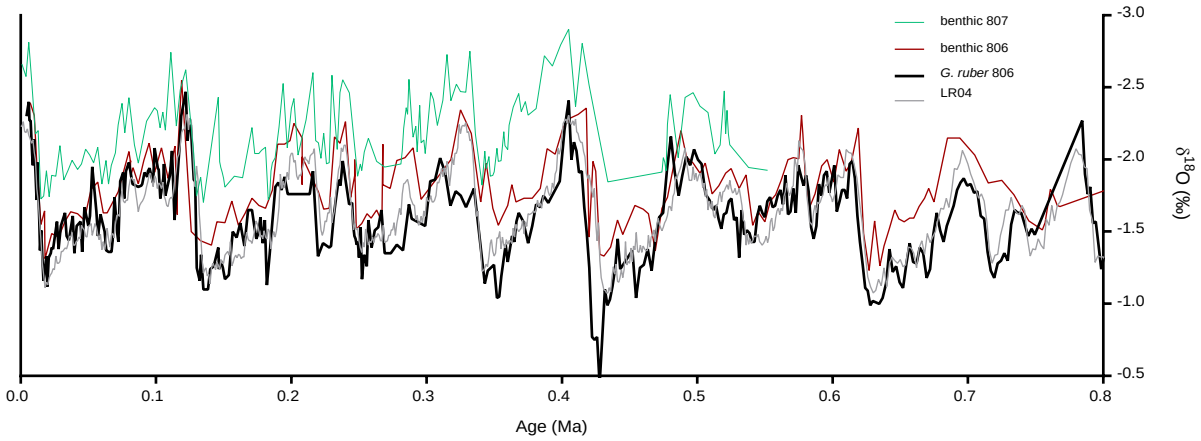
benthic 807
benthic 806
G. ruber 806
LR04
-3.0
-2.5
-2.0
-1.5
-1.0
-0.5
δ18O (‰)
0.0
0.1
0.2
0.3
0.4
0.5
0.6
0.7
0.8
Age (Ma)

Figure S3

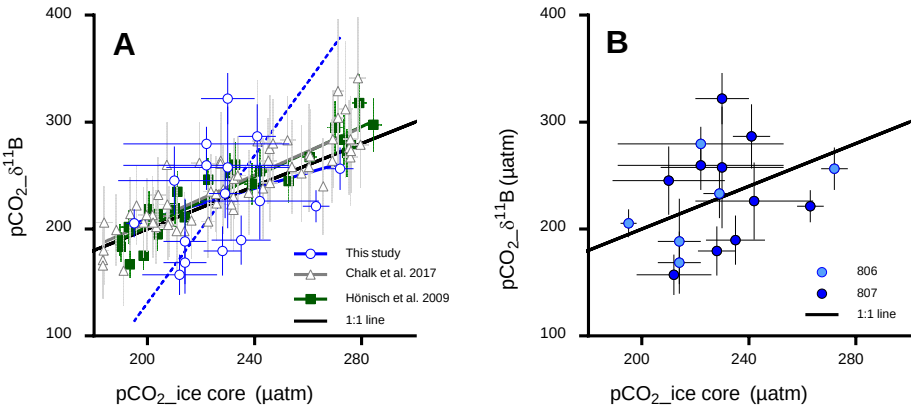
A
B
400
300
200
100
200
240
280
pCO2_δ11B
pCO2_δ11B (µatm)
pCO2_ice core (µatm)
This study
Chalk et al. 2017
Hönisch et al. 2009
1:1 line
806
807
1:1 line

Figure S4

References

Barker S., Greaves M. and Elderfield H.: A study of cleaning procedures used for foraminiferal Mg/Ca paleothermometry. Geochemistry, Geophys. Geosystems 4, 1–20, 2003.

Bian, N., & Martin, P. A.: Investigating the fidelity of Mg/Ca and other elemental data from reductively cleaned planktonic foraminifera. Paleoceanography, 25(2), 2010.

Brennan, S. T., Lowenstein, T. K., & Cendón, D. I. : The major-ion composition of Cenozoic seawater: The past 36 million years from fluid inclusions in marine halite. American Journal of Science, 313(8), 713-775, 2013.

Caves J. K., Jost A. B., Lau K. V. and Maher K.: Cenozoic carbon cycle imbalances and a variable weathering feedback. Earth Planet. Sci. Lett. 450, 152–163, 2016.

Chalk T. B., Hain M. P., Foster G. L., Rohling E. J., Sexton P. F., Badger M. P. S., Cherry S. G., Hasenfratz A. P., Haug G. H., Jaccard S. L., Martínez-García A., Pälike H., Pancost R. D. and Wilson P. A.: Causes of ice age intensification across the Mid-Pleistocene Transition. Proc. Natl. Acad. Sci., 201702143, 2017.

Coggon, R. M., Teagle, D. A. H., Smith-Duque, C. E., Alt, J. C., & Cooper, M. J.: Reconstructing past seawater Mg/Ca and Sr/Ca from mid-ocean ridge flank calcium carbonate veins. Science, 327(5969), 1114–1117. https://doi.org/10.1126/science.1182252, 2010.

Coggon, R. M., Teagle, D. A. H. and Dunkley Jones, T.: Comment on "What do we know about the evolution of Mg to Ca ratios in seawater?" by Wally Broecker and Jimin Yu. Paleoceanography 26, 2011.

DeFantle, M. S. and DePaolo, D. J.: Sr isotopes and pore fluid chemistry in carbonate sediment of the Ontong Java Plateau: Calcite recrystallization rates and evidence for a rapid rise in seawater Mg over the last 10 million years. Geochim. Cosmochim. Acta 70, 3883–3904, 2006.

Dekens, P. S., Lea, D. W., Pak, D. K. and Spero H. J.: Core top calibration of Mg/Ca in tropical foraminifera: Refining paleotemperature estimation. Geochemistry, Geophys. Geosystems 3, 1–29, 2002.

Delaney, M. L., Bé, A. W., & Boyle, E. A.: Li, Sr, Mg, and Na in foraminiferal calcite shells from laboratory culture, sediment traps, and sediment cores. Geochimica et Cosmochimica Acta, 49(6), 1327-1341, 1985.

Dickson A. G.: Thermodynamics of the Dissociation of Boric Acid in Potassium Chloride Solutions from 273.15 to 318.15 K. J. Chem. Eng. Data 35, 253–257, 1990.

Dickson, J. A. D.: Fossil echinoderms as monitor of the Mg/Ca ratio of Phanerozoic oceans. Science, 298(5596), 1222–1224. https://doi.org/10.1126/science.1075882, 2002.

Evans, D. & Müller, W.: Deep time foraminifera Mg/Ca paleothermometry: Nonlinear correction for secular change in seawater Mg/Ca. Paleoceanography 27, PA4205, 2012.

Evans, D., Sagoo, N., Renema, W., Cotton, L. J., Müller, W., Todd, J. A., Saraswati, P. K., Stassen, P., Ziegler, M., Pearson, P. N., Valdes, P. J., and Affek, H. P.: Eocene greenhouse climate revealed by coupled clumped isotope-Mg/Ca thermometry. Proceedings of the National Academy of Sciences, 115(6), 1174–1179. http://doi.org/10.1073/pnas.1714744115, 2018.

Evans, D., Wade, B. S., Henenhan, M., Erez, J., & Müller, W.: Revisiting carbonate chemistry controls on planktic foraminifera Mg/Ca: implications for sea surface temperature and hydrology shifts over the Paleocene–Eocene Thermal Maximum and Eocene–Oligocene transition. Climate of the Past, 12(4), 819-835, 2016.

Gothmann A. M., Stolarski J., Adkins J. F., Schoene B., Dennis K. J., Schrag D. P., Mazur M. and Bender M. L.: Fossil corals as an archive of secular variations in seawater chemistry since the Mesozoic. Geochim. Cosmochim. Acta 160, 188–208, 2015.

Gray, W. R., & Evans, D.: Nonthermal influences on Mg/Ca in planktonic foraminifera: a review of culture studies and application to the Last Glacial Maximum. Paleoceanography and Paleoclimatology, 34(3), 306-315, 2019.

Gray, W. R., Weldeab, S., Lea, D. W., Rosenthal, Y., Gruber, N., Donner, B., & Fischer, G.: The effects of temperature, salinity, and the carbonate system on Mg/Ca in Globigerinoides ruber (white): A global sediment trap calibration. Earth and Planetary Science Letters, 482, 607-620, 2018.

Greenop R., Hain M. P., Sosdian S. M., Oliver K. I. C., Goodwin P., Chalk T. B., Lear C. H., Wilson P. A. and Foster G. L.: A record of Neogene seawater δ11B reconstructed from paired δ11B analyses on benthic and planktic foraminifera. Clim. Past 13, 149–170, 2017.

Guillermic, M., Misra, S., Eagle, R., Villa, A., Chang, F., Tripati, A.,: Seawater pH reconstruction using boron isotopes in multiple planktonic foraminifera species with different depth habitats and their potential to constrain pH and pCO2 gradients. Biogeosciences, 17(13), 3487-3510, 2020.

Hemming N. G. and Hanson G. N.: Boron isotopic composition and concentration in modern marine carbonates. Geochim. Cosmochim. Acta 56, 537–543, 1992.

Henehan M. J., Foster G. L., Bostock H. C., Greenop R., Marshall B. J. and Wilson P. A.: A new boron isotope-pH calibration for Orbulina universa, with implications for understanding and accounting for 'vital effects.' Earth Planet. Sci. Lett. 454, 282–292, 2016.

Henehan M. J., Rae J. W. B., Foster G. L., Erez J., Prentice K. C., Kucera M., Bostock H. C., Martínez-Botí M. A., Milton J. A., Wilson P. A., Marshall B. J. and Elliott T. (2013) Calibration of the boron isotope proxy in the planktonic foraminifera Globigerinoides ruber for use in palaeo-CO2reconstruction. Earth Planet. Sci. Lett. 364, 111–122, 2013.

Hönisch, B., Allen, K. A., Lea, D. W., Spero, H. J., Eggins, S. M., Arbuszewski, J., deMenocal, P., Rosenthal, Y., D. Russel, a.: Elderfield, H.: The influence of salinity on Mg/Ca in planktic foraminifers–Evidence from cultures, core-top sediments and complementary d 18 O. Geochimica Et Cosmochimica Acta, 121, 196-213, 2013.

Hönisch, B., Eggins, S. M., Haynes, L. L., Allen, K. A., Holland, K. D., & Lorbacher, K.: Boron Proxies in Paleoceanography and Paleoclimatology, 2019.

Hönisch, B. and Hemming, N. G., Ground-truthing the boron isotope-paleo-pH proxy in planktonic foraminifera shells: Partial dissolution and shell size effects, Paleoceanography 19, 1–13, 2004.

Horita J., Zimmermann H. and Holland H. D.: Chemical evolution of seawater during the Phanerozoic: Implications from the record of marine evaporites. Geochim. Cosmochim. Acta 66, 3733–3756., 2002.

Johnstone, H. J., Lee, W., & Schulz, M.: Effect of preservation state of planktonic foraminifera tests on the decrease in Mg/Ca due to reductive cleaning and on sample loss during cleaning. Chemical Geology, 420, 23-36, 2016.

Kısakürek, B., Eisenhauer, A., Böhm, F., Garbe-Schönberg, D., & Erez, J.: Controls on shell Mg/Ca and Sr/Ca in cultured planktonic foraminiferan, Globigerinoides ruber (white). Earth and Planetary Science Letters, 273(3-4), 260-269, 2008.

Klochko K., Kaufman A. J., Yao W., Byrne R. H. and Tossell J. A.: Experimental measurement of boron isotope fractionation in seawater. Earth Planet. Sci. Lett. 248, 261–270, 2006.

Lee, K., Kim, T. W., Byrne, R. H., Millero, F. J., Feely, R. A., & Liu, Y. M.: The universal ratio of boron to chlorinity for the North Pacific and North Atlantic oceans. Geochimica et Cosmochimica Acta, 74(6), 1801-1811, 2010.

Lemarchand D., Gaillardet J., Lewin and Allégre C. J.: The influence of rivers on marine boron isotopes and implications for reconstructing past ocean pH. Nature 408, 951–954, 2002.

Lisiecki L. E. and Raymo M. E.: A Pliocene-Pleistocene stack of 57 globally distributed benthic δ18O records. Paleoceanography 20, 1–17, 2005.

Lueker, T. J., Dickson, A. G., & Keeling, C. D.: Ocean pCO2 calculated from dissolved inorganic carbon, alkalinity, and equations for K1 and K2: validation based on laboratory measurements of CO2 in gas and seawater at equilibrium. Marine chemistry, 70(1-3), 105-119, 2000.

Medina-Elizalde M. and Lea D. W.: The mid-pleistocene transition in the tropical pacific. Science 310, 1009–1012, 2005.

Misra, S., Greaves, M., Owen, R., Kerr, J., Elmore, A. C. and Elderfield, H.: Determination of B/Ca of natural carbonates by HR-ICP-MS. Geochemistry, Geophys. Geosystems 15, 1617–1628, 2014a.

Ni Y., Foster G. L., Bailey T., Elliott T., Schmidt D. N., Pearson P., Haley B. and Coath C.: A core top assessment of proxies for the ocean carbonate system in surface-dwelling foraminifers. Paleoceanography 22, 2007.

Nir O., Vengosh A., Harkness J. S., Dwyer G. S. and Lahav O.: Direct measurement of the boron isotope fractionation factor: Reducing the uncertainty in reconstructing ocean paleo-pH. Earth Planet. Sci. Lett. 414, 1–5, 2015.

Nürnberg, D., Bijma, J., & Hemleben, C.: Assessing the reliability of magnesium in foraminiferal calcite as a proxy for water mass temperatures. Geochimica et Cosmochimica Acta, 60(5), 803-814, 1996.
O'Brien C. L., Foster G. L., Martínez-Botí M. A., Abell R., Rae J. W. B. and Pancost R. D.: High sea surface temperatures in tropical warm pools during the Pliocene. Nat. Geosci. 7, 606–611, 2014.
Perez, F. F., & Fraga, F.: Association constant of fluoride and hydrogen ions in seawater. Marine Chemistry, 21(2), 161-168, 1987.
Pierrot, D., Lewis, E., & Wallace, D. W. R.: MS Excel program developed for CO2 system calculations. ORNL/CDIAC-105a. Carbon Dioxide Information Analysis Center, Oak Ridge National Laboratory, US Department of Energy, Oak Ridge, Tennessee, 10, 2006.
Raitzsch M. and Hönisch B.: Cenozoic boron isotope variations in benthic foraminifers. Geology 41, 591–594, 2013.
Raitzsch M., Bijma J., Benthien A., Richter K. U., Steinhoefel G. and Kučera M.: Boron isotope-based seasonal paleo-pH reconstruction for the Southeast Atlantic – A multispecies approach using habitat preference of planktonic foraminifera. Earth Planet. Sci. Lett. 487, 138–150, 2018.
Rausch, S., Böhm, F., Bach, W., Klügel, A., & Eisenhauer, A.: Calcium carbonate veins in ocean crust record a threefold increase of seawater Mg/Ca in the past 30 million years. Earth and Planetary Science Letters, 362, 215–224, 2013.
Rickaby, R. E. M. and Halloran, P.: Cool La Nina During the Warmth of the Pliocene?, Science, 307, 1948–1952, 2005.
Ridgwell A. and Zeebe R. E.: The role of the global carbonate cycle in the regulation and evolution of the Earth system. Earth Planet. Sci. Lett. 234, 299–315, 2005.
Russell, A. D., Hönisch, B., Spero, H. J., & Lea, D. W.: Effects of seawater carbonate ion concentration and temperature on shell U, Mg, and Sr in cultured planktonic foraminifera. Geochimica et Cosmochimica Acta, 68(21), 4347-4361, 2004.
Sosdian, S. M., Babila, T. L., Greenop, R., Foster, G. L., & Lear, C. H.: Ocean carbon storage across the middle Miocene: A new interpretation for the Monterey Event. Nature communications, 11(1), 1-11, 2020.
Sosdian, S. M., Greenop R., Hain M. P., Foster G. L., Pearson P. N. and Lear C. H.: Constraining the evolution of Neogene ocean carbonate chemistry using the boron isotope pH proxy. Earth Planet. Sci. Lett. 498, 362–376, 2018.
Sutton J. N., Liu Y.-W., Ries J. B., Guillermic M., Ponzevera E. and Eagle R. A.: δ11B as monitor of calcification site pH in divergent marine calcifying organisms. Biogeosciences 15, 1447–1467, 2018.
Tyrrell, T., & Zeebe, R. E.: History of carbonate ion concentration over the last 100 million years. Geochimica et Cosmochimica Acta, 68(17), 3521-3530, 2004.
Yu, J., Elderfield, H., Greaves, M., & Day, J.: Preferential dissolution of benthic foraminiferal calcite during laboratory reductive cleaning. Geochemistry, Geophysics, Geosystems, 8(6), 2007a.
Zachos J. C., Dickens G. R. and Zeebe R. E.: An early Cenozoic perspective on greenhouse warming and carbon-cycle dynamics. Nature 451, 279–283, 2008.